Static Friction in a Cable-Driven Transmission—Modeling and Identification of Load Effects

Giovanni Torres-Charry [1],* and **Juan-Bernardo Gómez-Mendoza** [2]

1. Mechanical Engineering Faculty, Universidad Tecnológica de Pereira, Pereira 660003, Colombia
2. Department of Electrical, Electronic and Computer Engineering, Universidad Nacional de Colombia, Manizales 170002, Colombia; jbgomezm@unal.edu.co
* Correspondence: gtorres@utp.edu.co

Abstract: Although many friction models have been developed by various researchers over the years, a general model does not exist yet. In this article, we present the work that was developed to identify and propose an empirical model that represents the behavior of friction in a cable-driven transmission. We designed and built a test bench that allowed us to study the incidence of friction as evidenced by the type of cable thread, the dimensions of the pulley and the capstan and the application of an external load for pulley-cable type transmissions in a variety of configurations. The results obtained show a marked influence of the external load on friction behavior. Based on these results, we propose a friction model that involves the external load and the transmission ratio. During the validation of the model, it was found that the proposed model reproduced the friction behavior better than the LuGre model, obtaining errors up to 44% lower, mainly for high loads and low speeds.

Keywords: cable-driven; transmission; friction; load; modeling; identification

1. Introduction

In the past decades, many researchers have worked on modeling and experimental identification of the friction phenomenon [1–9]. These models and some of their variations have been widely used for friction modeling in industrial robots [10–15]. However, most of these models only consider the relative speed between the interacting surfaces in their formulation. On the other hand, depending on the type of transmission, there is a complex interaction of components in the joint of a robot, such as pinions, shafts, cables or bearings that rotate or slide at different speeds; hence, a general model can hardly include all these behaviors for the entire spectrum of possible transmission types.

Empirically motivated friction models have been developed over time by observing the phenomenon of friction, some of which have demonstrated good performance in many applications, including robotics [16–19]. These empirical friction models consider a set of states X and parameters Φ, which are arranged in functions f_i. These models are then described as the sum of N functions f_i; in this way, the behavior of friction can be described by Equation (1).

$$F_f(X, \Phi) = \sum_{i=1}^{N} f_i(X, \Phi) \tag{1}$$

The structure of the models is influenced by the choice of X. A typical choice is $X = \left[z, \theta, \dot{\theta}\right]$, where z is a state variable that is related to the dynamic behavior of friction, θ is a generalized variable (traditionally position) and $\dot{\theta} = \frac{d\theta}{dt}$ [20].

Among the empirical models, the LuGre model [21,22] is a common choice in the industrial and robotics community. Described by Equation (2), the LuGre model uses the state variable z, which is interpreted as the average deformation of the bristles between

the contact surfaces. Seven parameters are used to describe the LuGre model, as shown in Table 1.

$$T_f = \sigma_0 z + \sigma_1 \dot{z} + \sigma_2 \dot{\theta}$$

$$\dot{z} = \dot{\varphi} - \sigma_0 \frac{|\dot{\theta}|}{g(\dot{\theta})} z \tag{2}$$

Table 1. LuGre model parameters.

Static Parameters	
F_C	Coulomb friction
F_S	Static friction (stiction)
σ_2	Viscous friction coefficient
α	Shape factor
$\dot{\theta}_s$	Stribeck velocity
Dynamic Parameters	
σ_0	Stiffness of the bristles
σ_1	Damping of the bristles

The function $g(\dot{\theta})$ captures the decrease in friction at low velocities with increasing speed (θ). The function $g(\dot{\theta})$ is generally modeled by Equation (3).

$$g(\dot{\theta}) = F_c + (F_s - F_c)e^{-\left|\frac{\dot{\theta}}{\dot{\theta}_s}\right|^{\alpha}} \tag{3}$$

According to the structure of empirical friction models (Equation (1)), the LuGre model is defined by two states $X = \left[z, \dot{\theta}\right]$ and seven parameters, four of which are static $\Phi_s = \left[F_c, F_s, \dot{\theta}_s, \sigma_2\right]$ and three of which are dynamic $\Phi_d = [\sigma_0, \sigma_1, \alpha]$. As mentioned before, the LuGre model depends only on z and $\dot{\theta}$; however, some authors have established the influence of other variables, such as temperature and external load, on friction behavior [22–24]. These works have been carried out on manipulator robots with gear transmissions. Taking into account the increasing use of cable transmissions in robot manipulators and devices that must interact with humans [25–29], it is important to obtain data on the behavior of friction in this type of transmission; in addition, a friction model consistent with actual experiments is required for appropriate simulation, design and evaluation.

There is some work related to the determination and modeling of friction in cable-driven parallel robots. For example, Miyasaka [30,31] developed a model of Coulomb cable-pulley interaction and viscous friction based on experimental measurements; the model and experimental procedures can be applied to cable-driven systems with structure, tension, load and cable and pulley parameters similar to RAVEN II [32]. Choi [33] proposed a Dahl friction model to predict stress during fast transitions in cable-driven parallel robots; then, the Dahl equation of friction was derived for a combination of pulleys connected in series. Lee [34] proposed a friction analysis method according to a claim and an experimental method for friction analysis presented by him; the correlation between pretension and friction is estimated by analysis. However, the constructive and operating characteristics of the systems evaluated in these works are different from those of a cable-pulley-type transmission for an industrial-type robotic arm, such as the one that concerns us in this work. Cable-driven industrial robotic arms typically have larger pulleys than those used in parallel robots. Also, there are typically multiple turns of cable winding on the capstan, and they run at higher speeds. On the other hand, these works also do not include the effect of the payload on the friction behavior.

This work addresses the determination of static friction in a cable-driven transmission, including the effect of a payload. The experiments are performed on a test bench designed

and built for this purpose at Universidad Tecnológica de Pereira, in partnership with Universidad Nacional de Colombia [35]. The test bench is loosely based on the articulations of a Barrett WAM arm created at the Massachusetts Institute of Technology [36]. The payload of the test bench is provided on the transmission shaft by a perforated disc and pairs of masses assembled on the disc. The distribution of the masses in the disc allows several configurations of the payload (external load and external torque). Three external load configurations, two transmission ratios and two types of cable threading are examined. From the empirical observations, a useful model structure is proposed, with the form

$$\tau_f(X, \Phi) = \sum_{i=1}^{n} f_i(X, \Phi)$$
$$X = \left[\dot{\theta}_m, N, L_r\right]$$

(4)

where $\dot{\theta}_m$ is the input rotation speed of the transmission, N is the transmission ratio and L_r is the resulting relative external load applied perpendicular to the degree of freedom (DOF).

The remainder of this document is organized as follows: Section 2 presents the method used to estimate static friction on the test bench, along with the guidelines used during the experiments. In Section 3, the empirical analysis, modeling and validation are presented. Finally, Section 4 draws the conclusions and proposes future work.

2. Materials and Methods

2.1. Experimental Device

The determination of the friction behavior is carried out on the experimental test bench designed by Torres [35]. On the test bench, the transmission module is configured by a steel cable (a), a capstan system (b) and a pulley system (c). The payload for the tests is supplied to the shaft of the pulley system, using pairs of masses (d) assembled on the perforated disc (e) of the test bench (Figure 1).
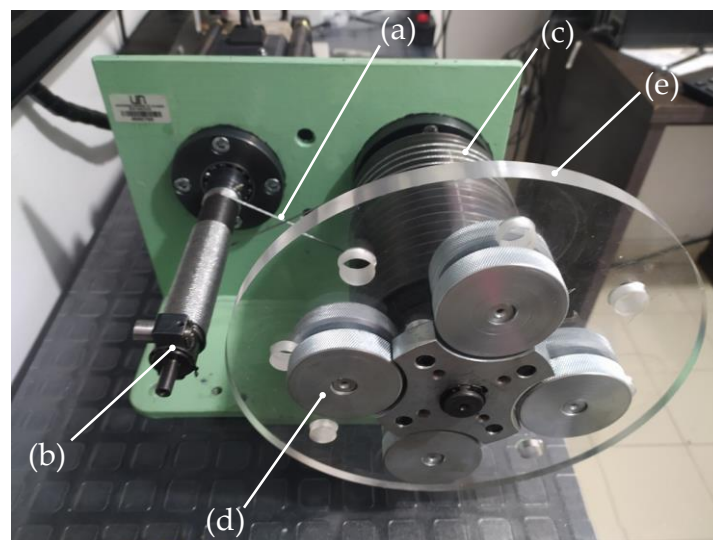

Figure 1. Details of the cable-driven transmission, disc and masses. (a) steel cable, (b) capstan system, (c) pulley system, (d) masses and (e) perforated disc.

To estimate the friction torque in the transmission, the reactive torque measurement was implemented in the motor. Unlike estimating torque from electrical power and motor rotational speed, the reactive torque measurement does not include the effect of the electrical power dissipated in the motor and the controller. Two S-type load cells, mounted at the rear of the motor and located equidistant from the motor shaft, restrict the motor body rotation and are used to measure the reactive force (Figure 2). With this configuration, one of the cells is subject to a compressive force, while the other is subject to a tensile force.
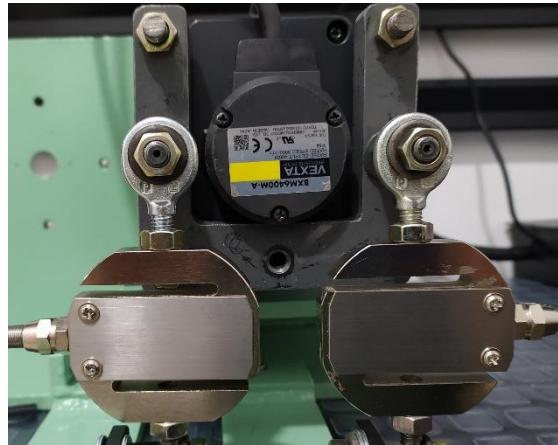
Figure 2. Details of the assembly of type S load cells.

From the point of view of mechanics, and according to the free-body diagram shown in Figure 3, the static equilibrium is given by Equation (5):

$$T_m - (F_1 \cdot L_1) - (F_2 \cdot L_2) = 0 \tag{5}$$

where T_m is the motor torque, F_1 and F_2 are the forces measured in the load cells and L_1 and L_2 are the distances between the point of application of the force and the geometric axis of rotation of the motor. In the test bench, L_1 was made equal to L_2, and then the T_m is calculated in Equation (6) as

$$T_m = (F_1 + F_2) \cdot L \tag{6}$$

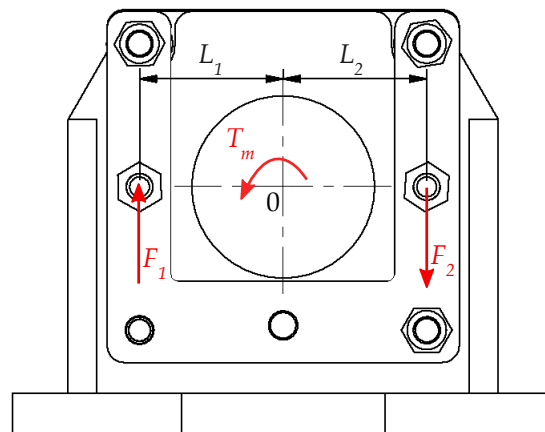with L as the distance between the load cells.

Figure 3. The free-body diagram for mounting the swing arm motor.

In the test bench tuning process, each load cell was calibrated, and creep adjustment relationships were also established.

The cable used in our experiments is a SAVA 1064 (Carl Stahl Low-Stretch) [37], featuring 49 strands (7 strands of 7 wires each) made of 304 stainless steel and an outer diameter of 1/16" (1.59 mm). The torsional stiffness of the transmission was modeled as a combination of three springs on each side of the pulley, as proposed by Werkmeister [38]. Figure 4 shows the variation of the torsional stiffness of the designed transmission, evaluated as a function of the transmitted torque, where *Tpr* is the preload tension in the cable. The torsional stiffness is high when the transmitted torque is close to zero. As the transmitted torque increases, the torsional stiffness of the transmission decreases.
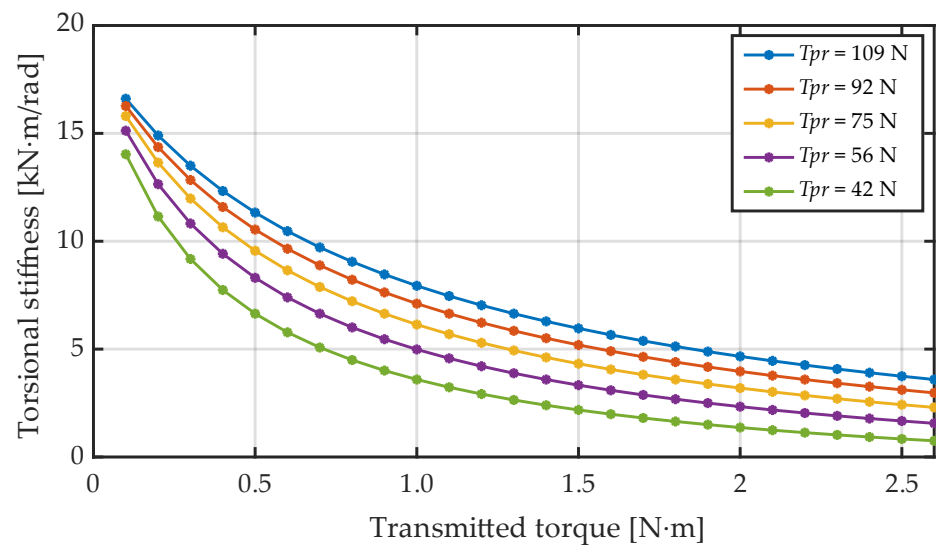
Figure 4. Effect of transmitted torque on transmission torsional stiffness.

Figure 5 shows the variation of the torsional stiffness of the transmission evaluated as a function of the applied preload, where T_L is the transmitted torque.
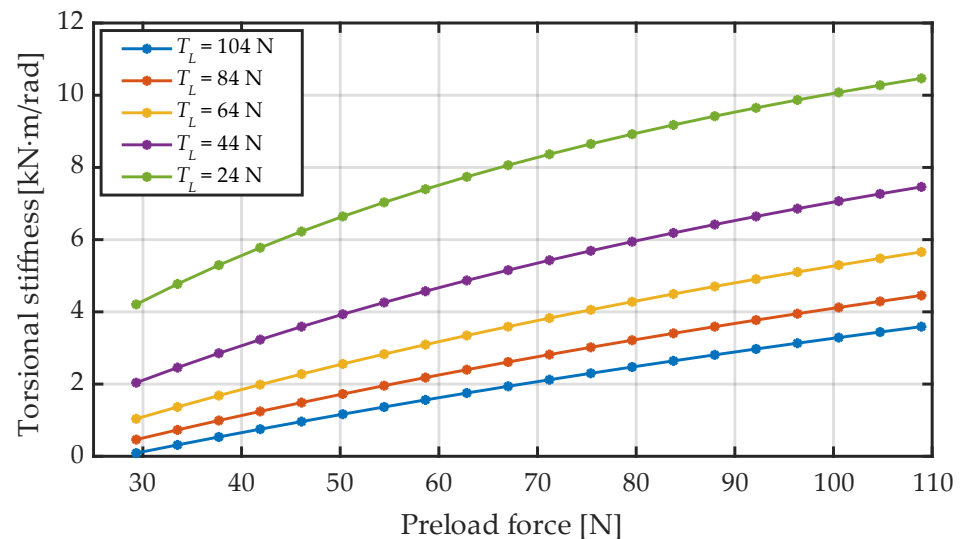

Figure 5. Effect of preload tension on transmission torsional stiffness.

To carry out the experiments, capstans and pulleys of different diameters and groove orientations were manufactured. Table 2 shows the physical characteristics of the elements used.

Table 2. Physical specifications of the transmission elements.

	Useful Length	Diameter	Weight	Inertia
	[mm]	[mm]	[N]	[kg·mm^2]
Capstan 25	140	25	7.95	65.39
Capstan 35	100	35	9.62	145.72
Pulley 75	105	75	25.46	1769.15
Pulley 104	140	104	23.49	4024.90

2.2. Transmission Model

The cable-driven transmission can be described using the simplified model of mechanical transmission (Figure 6) [36]; this model is governed by Equation (7):

$$T_M = \left[(J_M + J_1) + \left(\frac{J_2 + J_L}{N^2} \right) \right] \ddot{\theta}_M + \left(B_M + \frac{B_L}{N^2} \right) \dot{\theta}_M + \frac{T_L}{N} + T_{fs} \tag{7}$$

where T_M is the motor torque, T_L is the load torque, J_M is the motor inertia, J_L is the load inertia, J_1 is the capstan inertia, J_2 is the pulley inertia, N is the transmission ratio, B_M is the viscous damping coefficient of the motor, B_L is the viscous damping coefficient of the load, $\dot{\theta}_M$ is the speed of the motor, $\ddot{\theta}_M$ is the acceleration of the motor and T_{fs} quantifies the friction torque without considering the viscous component.
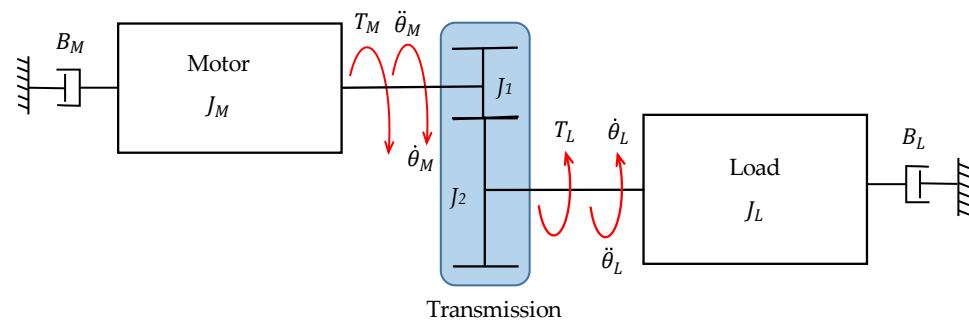

Figure 6. Schematic of the simplified model of the cable-driven transmission.

The identification of friction in the transmission was performed in a steady state. In the steady state, using pairs of balanced masses about the pulley axis (in this case the payload only implies an external load and not an external torque) and using the same type of bearings and grease for the capstan and the pulley, Equation (7) takes the form:

$$T_M = B_M \left(\frac{N^2 + 1}{N^2} \right) \dot{\theta}_M + T_{fs} \tag{8}$$

2.3. Guidelines for the Experiments

Friction identification was carried out offline. During the experiments, records of the position of the input shaft to the transmission and the forces in the load cells, the external force applied and the corresponding sampling time were kept. Data acquisition was done at 1 kHz ($T = 0.001$ s). The data of the angular position were filtered using wavelets [39,40], employing the Wavelet Toolbox of Matlab [41]. The wavelet chosen was of the Daubechies with 10 levels and universal threshold. Filtered data were used to calculate the rotational speed. The values of the forces in the load cells were used to calculate the reactive torque in the motor using Equation (6).

The motor control was used to move the input shaft at the desired speed (w_M), for which trapezoidal speed profiles were used at different positive and negative speeds. Data acquisition start times in the tests were adjusted to perform the measurements in the same physical position of the cable in the pulley and the capstan. Sampling times were adjusted to cover the same axial displacement of the cable over the pulleys; therefore, low-speed tests take longer to perform and collect data than high-speed tests. An example of the measurement of the position and reactive torque in the transmission is presented in Figure 7, for a speed of 1000 rpm in the motor. The data segment in the box in the figure corresponds to the linear change in position that is used to calculate joint velocity.
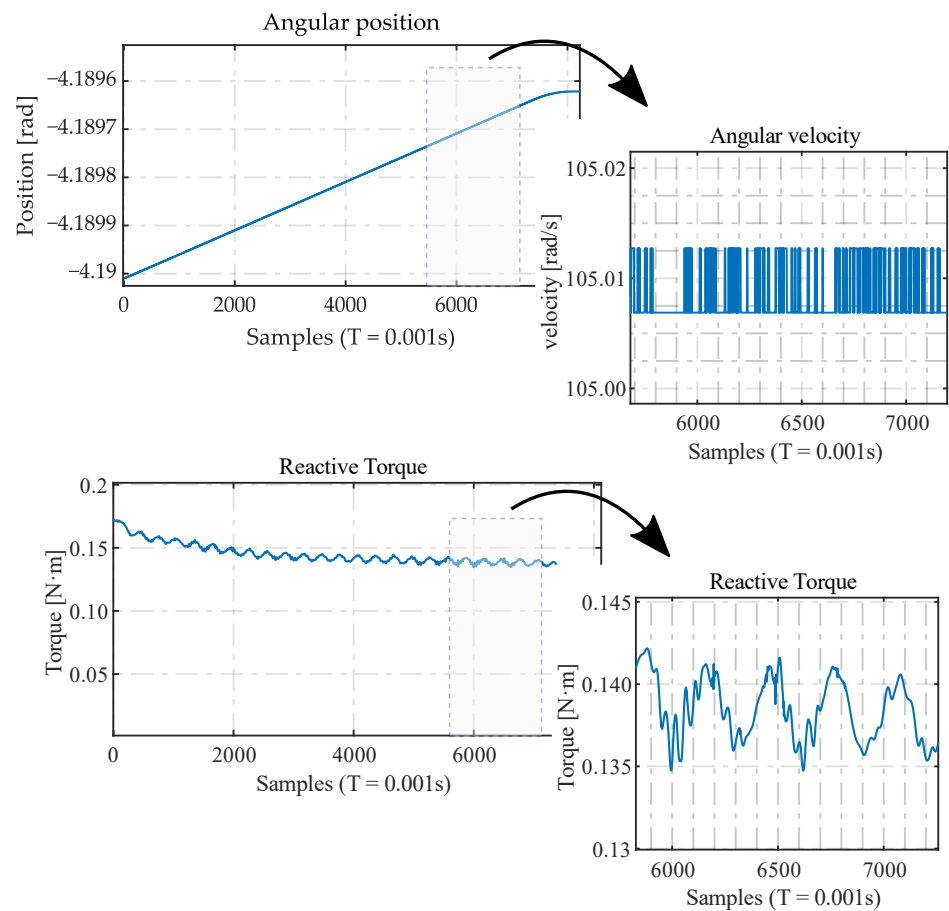
Figure 7. Measurement of the position and reactive torque in the transmission without external load, for a speed of 1000 rpm (105 rad/s) in the motor.

To reduce the temperature variation in the bearings, the transmission is operated for 30 min before starting the tests. After each data measurement, the transmission returns to its initial position and a time interval equal to the double-time used in the previous test is waited before carrying out the next test. The bearings used in all cable-driven configurations were SKF 61905 deep groove ball bearings. The same type of cable was used in all tests: SAVA 1064 [38], featuring 49 strands (7 strands of 7 wires each) made of 304 stainless steel and an outer diameter of 1/16" (1.59 mm).

Several configurations of the transmission were planned to identify the effect of certain construction and operating parameters on the friction behavior. Those configurations are set up by varying the diameter of the capstans and pulleys, varying the use of grooves in the pulleys, changing the type of cable threading and applying an external load (Table 3). For each type of test, 20 runs are performed non-consecutively. The speed used at the input of the test bench ranges from 1 rad/s to 105 rad/s (10–1000 rpm). The average velocity w_M and torque $T(w_M)$ in each test, given as ordered pairs $[T(w_M), w_M]$, shape the friction velocity map. The torque and speed pairs during the constant speed stage of the trajectory were averaged and used to build the friction speed map and the friction model.

Table 3. Transmission configurations evaluated.

Configuration	Capstan	Pulley	Thread	Disc	Masses
C25P104GP	25 mm	104 mm	P	No	0
C25P104GP-D	25 mm	104 mm	P	Yes	0
C25P104GP-D2M	25 mm	104 mm	P	Yes	2
C25P104GP-D4M	25 mm	104 mm	P	Yes	4
C25P104GX	25 mm	104 mm	X	No	0
C25P104GX-D	25 mm	104 mm	X	Yes	0
C25P104GX-D2M	25 mm	104 mm	X	Yes	2
C25P104GX-D4M	25 mm	104 mm	X	Yes	4
C35P75GX	35 mm	75 mm	X	No	0
C35P75GX-D	35 mm	75 mm	X	Yes	0
C35P75GX-D2M	35 mm	75 mm	X	Yes	2
C35P75GX-D4M	35 mm	75 mm	X	Yes	4

3. Results and Discussion

First, the influence of the type of cable thread on the friction behavior is measured, and then the effect of the external load on the friction behavior is measured. Based on the results obtained in the experiments, an empirical equation is proposed that involves the effect of speed, the external load and the transmission ratio.

For the experiments in which the effect of loading was evaluated, a perforated disc and pairs of balanced masses attached to the disc were used; this assembly is attached at the end of the pulley shaft (Figure 1). Table 4 shows the inertial characteristics of the perforated disc and the masses.

Table 4. Inertial specifications of the perforated disc and the additional masses.

	Weight	Inertia
	[N]	[kg·mm^2]
Perforated disc	11.28	3790.2
Disc and one pair of masses	21.09	12,910.6
Disc and two pairs of masses	30.90	22,031.1

The load on the bearings results from the effect of the weight of the transmission elements (shafts, capstan and pulley), the tension in the cable and the external load applied to the transmission. Particularly in the configurations of the developed transmission, the external load and weight are applied in cantilever, so their effect on the bearings that support each axis depends on the dimensions of the transmission for each configuration. Figures 8 and 9 show the free-body diagrams for the pulleys and the capstan; in bearings A and B there are reactive forces in the y and z directions; it is assumed that the weight of the element is concentrated in the center of gravity (*cg*) and directed in the negative y-direction, and at point D it is assumed that the resultant force of the cable is applied in the z-direction and the external load is applied at point E. The dimensions of the pulleys and capstans are given in Table 5.
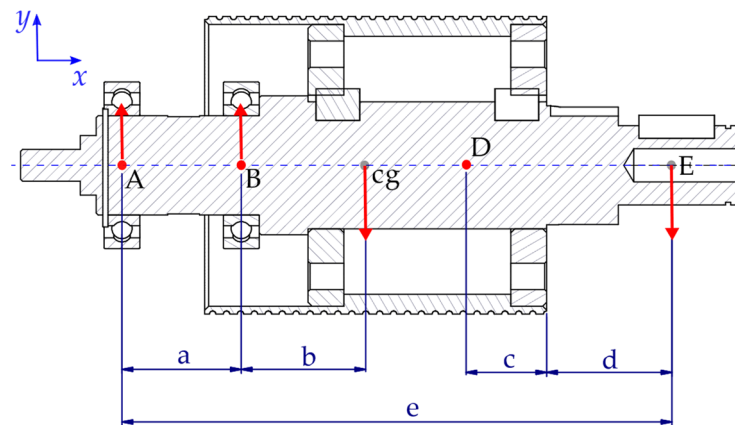
Figure 8. Free-body diagram of the transmission pulleys of the test bench: (A), (B) bearings position, (cg) center of gravity, (D) point of application of the cable force, (E) external force application point, and (a–e) shaft dimensions.
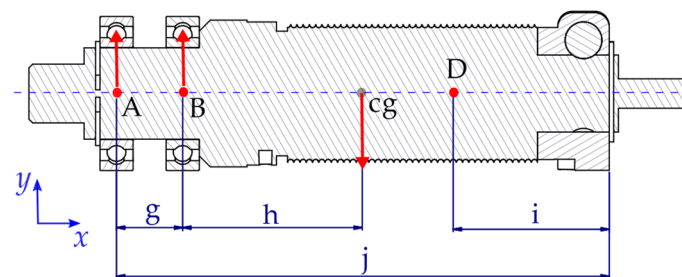

Figure 9. Free-Body Diagram of the Test Bench Transmission capstans: (A), (B) bearings position, (cg) center of gravity, (D) point of application of the cable force, and (g–j) shaft dimensions.

Table 5. Dimensions of the capstans and pulleys.

Element	Dimensions [mm]				
	g	**h**	**i**	**j**	
Capstan 35 mm	18	52	41	134	
Capstan 25 mm	18	80	60	195	
	a	**b**	**c**	**d**	**e**
Pulley 75 mm	30	31	31	32	139
Pulley 104 mm	30	70	46	20	190

3.1. Friction in a Cable-Driven Transmission and Effect of the Cable Threading

In this phase, two base configurations were used: C25P104GP and C25P104GX. Both consist of a 25 mm diameter capstan and a 104 mm diameter pulley, with guide grooves on their surface but different pulley groove directions. Table 2 shows the physical characteristics of the elements. The bearings were lubricated with Timken premium industrial grease LC2, with a nominal viscosity of 200–240 cSt at 40 °C.

To establish whether there is a significant difference in friction behavior based on the type of cable thread, experiments were carried out for the same physical configuration with different threads: C25P104GP (parallel cable threading) and C25P104GX (eight cable threading). Figures 10–12 show the results obtained in the test.
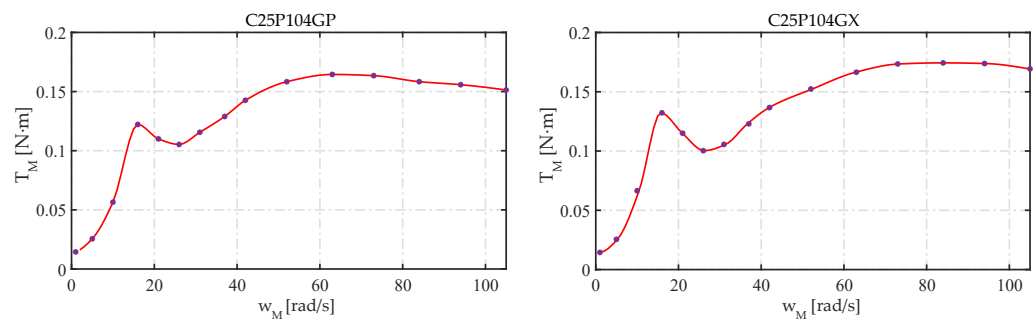
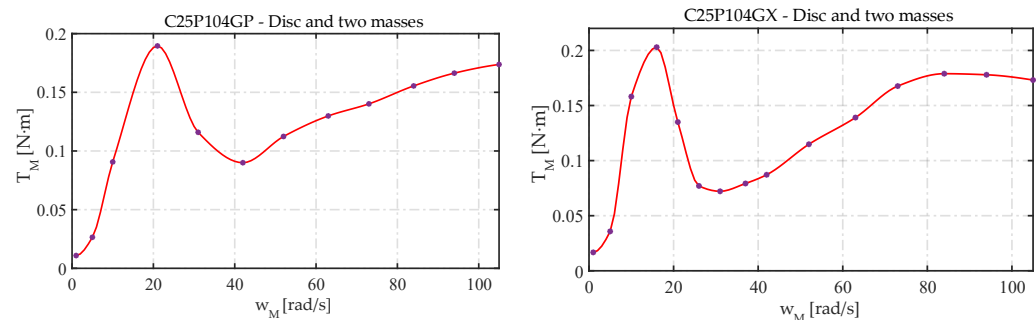**Figure 10.** Speed−torque curves for the C25P104GP and C25P104GX configurations.

Figure 11. Speed−torque curves for the C25P104GP-D2M and C25P104GX-D2M configurations.
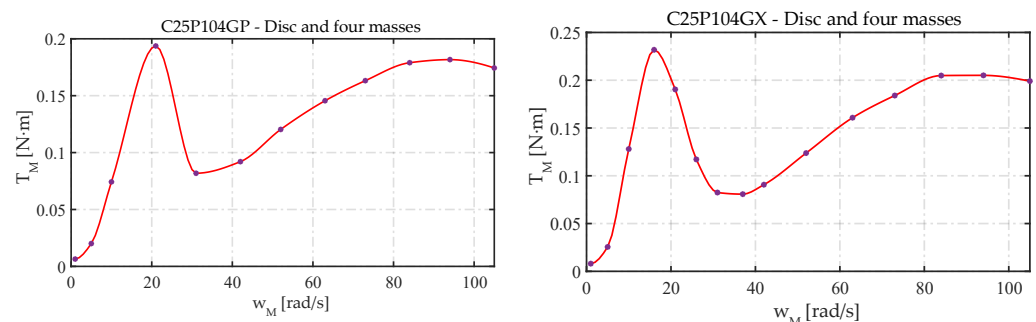

Figure 12. Speed−torque curves for the C25P104GP-D4M and C25P104GX-D4M configurations.

The curves obtained present a similar profile between configurations, with a slight difference in the values. In the cases in which an external load was applied, it was observed that a peak develops between 15 and 21 rad/s and a valley develops between 30 and 40 rad/s; then, friction begins to grow steadily and nonlinearly with a decay after 80 rad/s. Peak values are higher for eight threading conditions, while valley values are similar.

It was expected that by having lower loads on the shafts, which are transmitted to the bearings, the friction values for the eight threading conditions would be much lower than those for the parallel threading conditions. However, the behavior obtained is similar; this can be explained by the fact that in eight threading, there is a more marked friction effect between the cable and the grooves than in parallel threading. This effect is due to the cable being threaded in an eight-shape, where the grooves on the surface of the pulley must be opposite to the grooves of the capstan, which, in turn, causes the cable at both the entrance and the exit of the capstan and the pulley to rub sideways against the groove. The experiments in this work were carried out with a distance between the centers of 150 mm. For the eight-shape threading, it should be noted that if the distance between centers decreases, so will the resulting load of the cable on the shaft, likely causing a lower value of friction in the bearings and therefore, a lower total value of friction. The latter will be tested in future work.

3.2. Friction in a Cable-Driven Transmission, Effect of the Transmission Ratio

Due to the lower loads on the driveshafts, eight threading is preferred over parallel threading. In this phase, testing was done for configurations using eight threading: C35P75GX and C25P104GX. C35P75GX consists of a 35 mm diameter capstan and a 75 mm diameter pulley. Figures 13–16 show the results attained in the experiment.
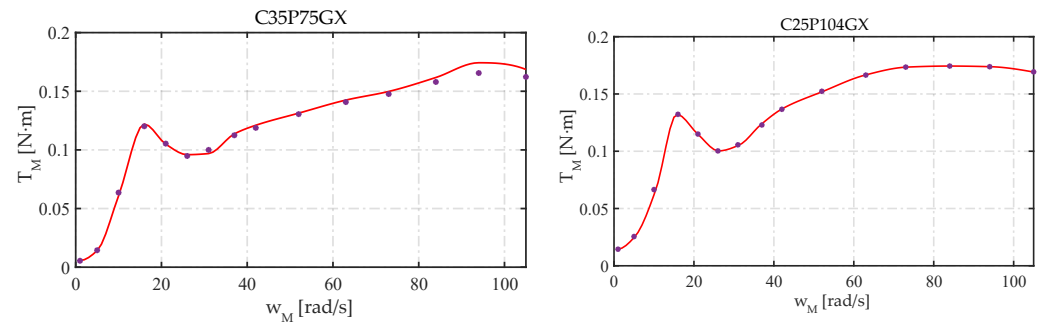

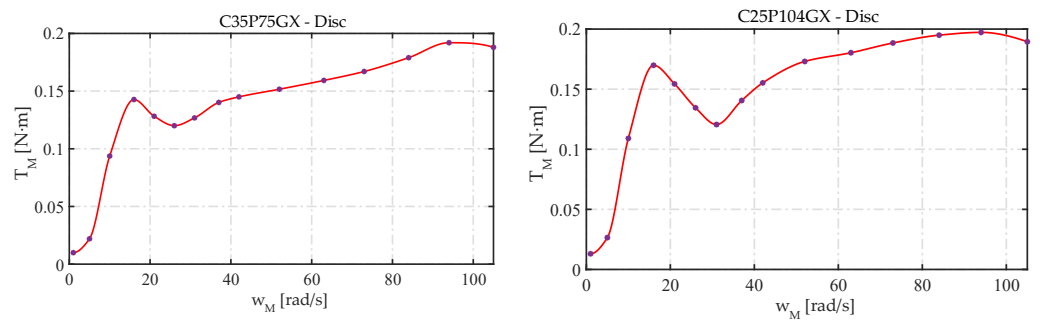**Figure 13.** Speed−torque curves for the C35P75GX and C25P104GX configurations.

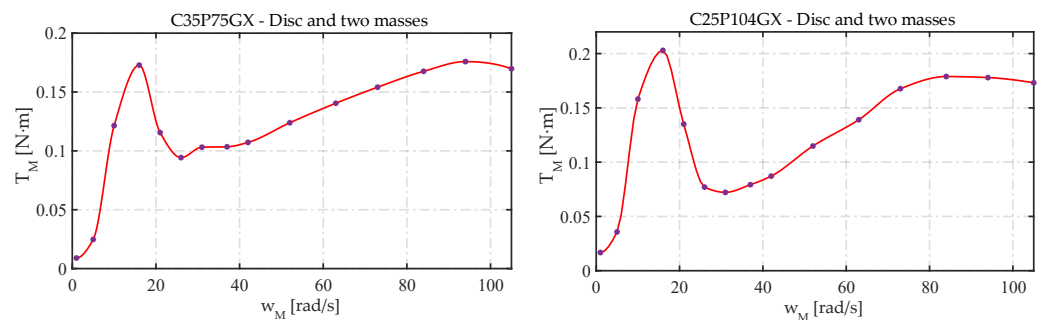**Figure 14.** Speed−torque curves for the C35P75GX-D and C25P104GX-D configurations.

Figure 15. Speed−torque curves for the C35P75GX-D2M and C25P104GX-D2M configurations.
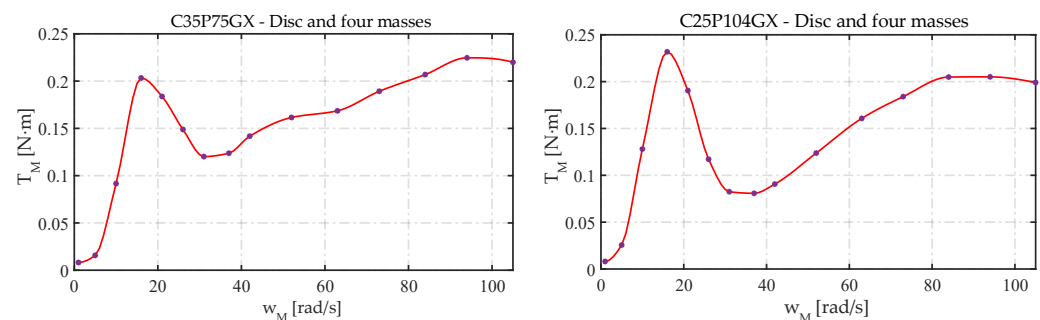

Figure 16. Speed−torque curves for the C35P75GX-D4M and C25P104GX-D4M configurations.

As in previous tests, the curves obtained present a similar profile between configurations. In the cases in which external load was applied, it is observed that a peak develops

between 15 and 21 rad/s and a valley develops between 30 and 40 rad/s; then, the friction begins to grow steadily and nonlinearly with a decay after 80 rad/s. The values in the peaks are higher for the C25P104GX configurations, while the values in the valleys are higher for the C35P75GX configurations. Recognizing that there may be an effect due to variables that are not being considered, the difference in the values of the peaks and valleys of the friction curve seem to be related to the applied external load, which, for the C25P104GX configuration, is positioned further away from the transmission bearings. Figures 17 and 18 show the friction behavior for the cases evaluated in the C35P75GX and C25P104GX configurations, respectively.
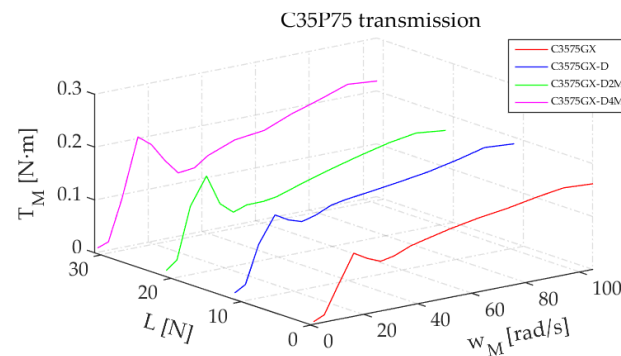

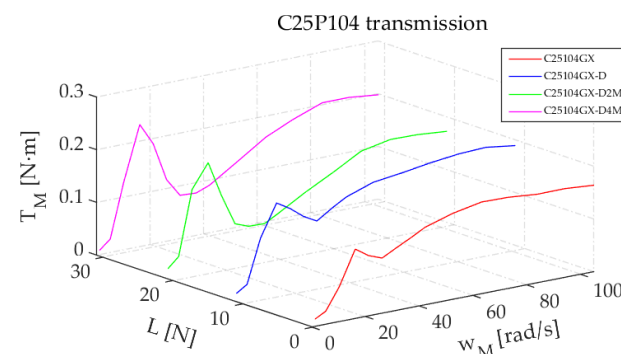**Figure 17.** Friction torque variation as a function of speed and external load for the C35P75GX configuration.

Figure 18. Friction torque variation as a function of speed and external load for the C25P104GX configuration.

3.3. Identification of Friction in Cable-Driven Transmission Based on the LuGre Model

The LuGre model is one of the most used in the robotics community; therefore, a first approximation of the friction model evaluated for cable-driven transmission is based on this model. Starting from the static LuGre model, the identification task consists of determining the parameters of the model. The parameters identified for the configurations evaluated are presented in Tables 6 and 7.

Table 6. Static parameters identified for the LuGre model (C35P75GX).

F_c [N·m]	F_s [N·m]	$\dot{\theta}_s$ [rad/s]	F_v [N·m·s/rad]	α
0.107	$3.367 \cdot 10^{-7}$	8.422	$7.596 \cdot 10^{-4}$	2

Table 7. Static parameters identified for the LuGre model (C25P104GX).

F_c [N·m]	F_s [N·m]	$\dot{\theta}_s$ [rad/s]	F_v [N·m·s/rad]	α
0.112	$1.405 \cdot 10^{-4}$	7.360	$7.161 \cdot 10^{-4}$	2

Figure 19 shows the friction profile determined for the static LuGre model with the estimated parameters for the C35P75GX-D4M configuration.
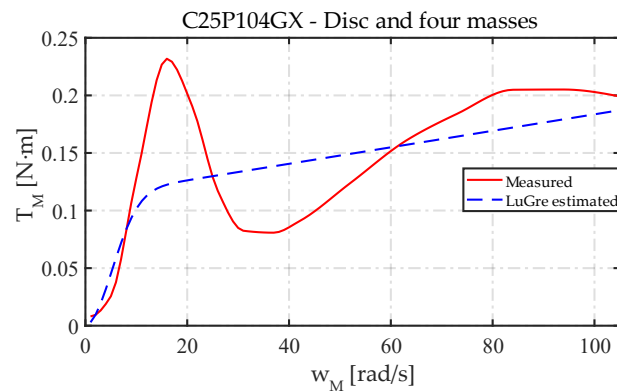

Figure 19. Static friction torque estimated using the LuGre model for the C35P75GX-D4M configuration.

The effect of the application of external load on the friction behavior (peaks and valleys) could not be adequately reproduced using the static LuGre model nor, presumably, by any model that does not explicitly involve the effect of external load. Figures 20 and 21 show the absolute value of the identification error when using the LuGre model for the C35P75GX configurations and C25P104GX configurations, respectively.

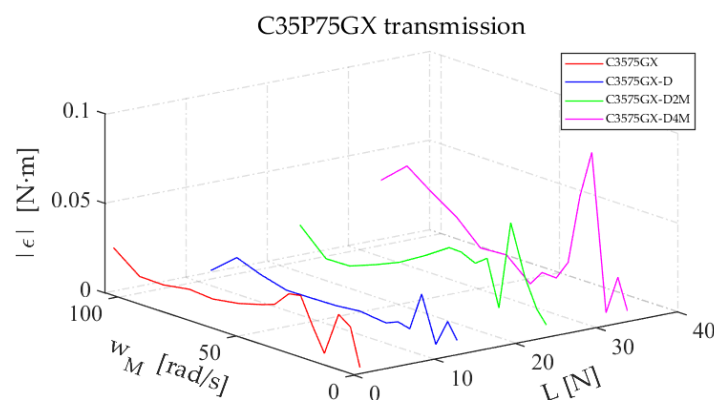**Figure 20.** Absolute error when using static LuGre model for C35P75GX configurations.
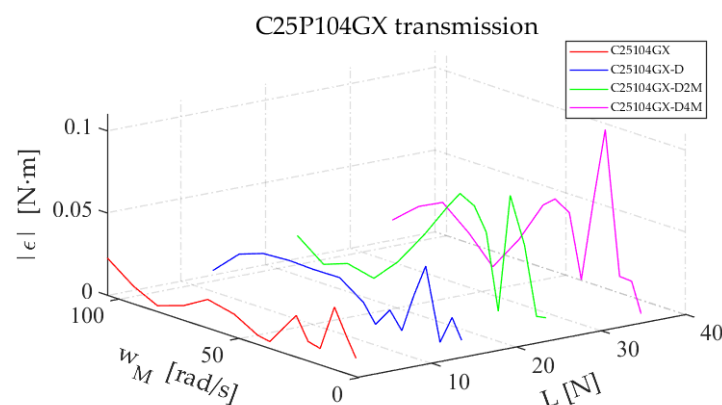

Figure 21. Absolute error when using static LuGre model for C25P104GX configurations.

3.4. Identification of Friction in Cable-Driven Transmission and Proposed Empirical Model

In addition to the rotation speed, the proposed alternative empirical model considers the effect of the transmission ratio and external loads.

3.5. External Load on the Transmission

For the friction model, we propose the use of the relative external load L_r, which is calculated by Equation (9):

$$L_r = \frac{\sum R_l}{\sum R_w} \tag{9}$$

where R_l is the reaction force in each bearing of the pulley for the evaluated configuration due to the weight of its own elements, the external loads and the tension in the cable and R_w is the reaction in each bearing of the transmission due only to the weight of the elements (without external loads).

3.6. Transmission Ratio N

The transmission ratio *N* causes the pulley to rotate at a speed *N* times slower than the capstan. Speed has a direct effect on viscous friction, so it is expected that the contribution made from the pulley will differ from the contribution made from the capstan; however, according to Equation (8), in which it is assumed that the viscous friction coefficient of the grease is the same in the capstan and the pulley, the difference in the total contribution of viscous friction for transmission ratios greater than 10 is less than 1% when calculated with input speed rather than individually for the pulley and the capstan.

3.7. Empirical Model

The main objective of the developed empirical model is to include in its formulation the effect of external load in such a way that the model can better approximate the behavior of friction in cable-driven transmissions.

It is known that friction is related to the interaction between surfaces in contact. One of the first phenomena observed by Coulomb was that friction varies according to the applied load. Applying external load to the test bench would change the behavior of the Coulomb friction component, the static friction component and the performance of the lubricant.

The results of the tests carried out reveal that Coulomb friction demonstrates non-linear behavior with increasing external load and speed. On the other hand, due to the design of the test equipment, the applied external load could influence the preload of the bearings, their fits and their tolerances.

The structure of the proposed model is presented in Equation (10):

$$\tau_f(X^*, \Phi) = \sum_{i=1}^{n} f_i(X^*, \Phi)$$
$$X^* = \left[\dot{\theta}_m, \, N, \, L_r \right] \tag{10}$$

where $\dot{\theta}_m$ is the input rotation speed of the transmission, *N* is the transmission ratio and L_r is the resulting relative external load applied perpendicular to the DOF.

Starting from the structure of the LuGre model, the measurements carried out support the proposal of the following model:

$$T_f\left(\dot{\theta}, N, L_r\right) = \left[(F_c + F_c \cdot L_r)\dot{\theta}^\delta + \left(F_s + (F_c + F_c \cdot L_r)\dot{\theta}^\beta \right) e^{-\left| \frac{\dot{\theta}}{\theta_s} \right|^\alpha} \right] \mathrm{sgn}(\dot{\theta}) + F_v \cdot \left[\left(\frac{N^2 + 1}{N^2} \right)\dot{\theta} + \left(\frac{\dot{\theta}}{L_r} \right)^\gamma \right] \tag{11}$$

The proposed model involves the parameters $\Phi = \left[F_c, F_s, \dot{\theta}_s, F_v, \, \delta, \beta, \alpha, \gamma \right]$. The parameters $F_c, F_s, \dot{\theta}_s, F_v$ and α have the same meaning as they do in the LuGre model; β and γ are shape factors used to implement the change of friction as a function of external load and speed.

The first term of Equation (11) quantifies the variation of Coulomb friction as a function of external load and speed. The second term quantifies the decrease in friction with increasing speed at low speeds (like the Stribeck effect); this term also includes the effect of external load and speed on increasing Coulomb friction. The last term quantifies viscous

friction as a function of speed, transmission ratio, the inverse effect of external load on the viscous friction coefficient of the grease and its non-Newtonian behavior. In the development of the model, the effect of temperature was not considered and there may be some difference in temperature in the transmission between tests; however, the tests were carried out whilst trying to limit the temperature gradient in the bearings and their effect on the grease. Aerodynamic drag was not evaluated when adding masses to the disc; therefore, it was not explicitly included in the model.

3.8. Empirical Model Validation

For the validation of the proposed friction model, a new set of experiments was developed, for which the same procedure used to obtain the data in the experimental phase was followed. The model parameters were identified using the data sets obtained in the experimental phase and using global search algorithms (Global Search) implemented in Matlab.

The measured values were compared with the values obtained from the proposed model (Equation (11)). In Figure 22, the behavior of friction, calculated using the proposed model and the values obtained experimentally, is compared for the C25P104GX-D4M configuration.
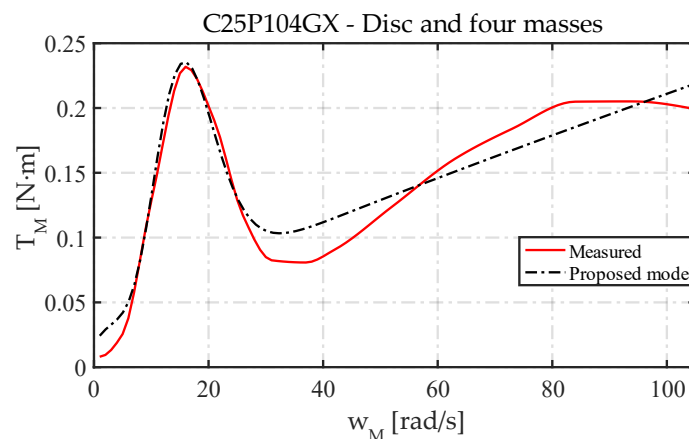

Figure 22. Static friction torque estimated using the model proposed for the C25P104GX-D4M configuration.

Figures 23 and 24 show the value of the absolute identification error when using the model proposed for the C35P75GX and C25P104GX configurations.
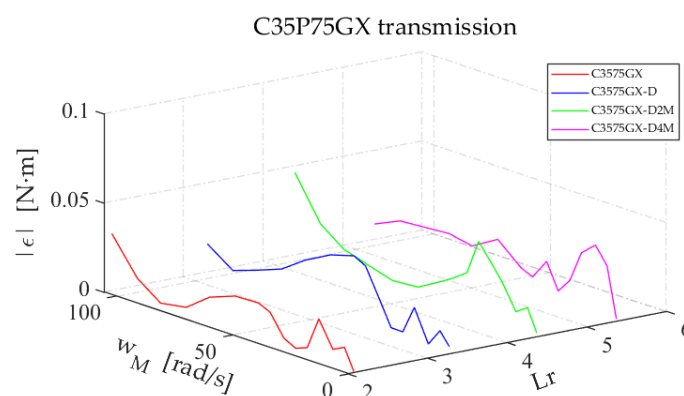

Figure 23. Absolute error when using the model proposed for the C35P75GX configurations.
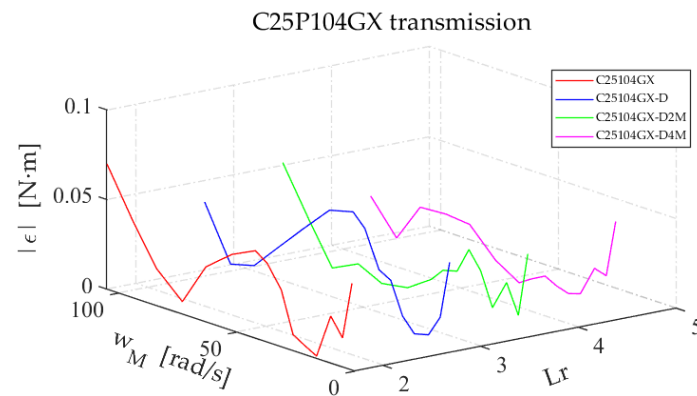
Figure 24. Absolute error when using the model proposed for the C25P104GX configurations.

Although the proposed model does not completely reproduce the friction behavior for the evaluated cable-driven transmissions, it presents lower values for the absolute error when compared with the LuGre model, mainly at low speeds and high external loads; therefore, it could be considered a better alternative. Table 8 presents a summary of the errors obtained with the proposed model and its comparison with the LuGre model.

Table 8. Summary of errors of the proposed friction model compared to the LuGre model.

	Friction Moment (N·m)				
Transmission	Measured	Proposed		LuGre	
	Value	Model	Error	Model	Error
C35P75GXD	0.1427	0.1268	11.1%	0.1185	17.0%
C35P75GXD2m	0.1728	0.1507	12.8%	0.1168	32.4%
C35P75GXD4m	0.2023	0.1740	14.0%	0.1167	42.3%
C25P104GXD	0.1700	0.1679	1.2%	0.1226	27.9%
C25P104GX2m	0.2030	0.1951	3.9%	0.1226	39.6%
C25P104GXD4m	0.2318	0.2260	2.5%	0.1226	47.1%

4. Conclusions

Although the LuGre model is the most widespread in the friction modeling and simulation literature due to its use in many applications and its simplicity of implementation, its use to quantify friction in cable-driven transmissions should be reviewed. In this work, a friction model for the cable-driven transmission is proposed that includes the effect of the external load and the transmission ratio.

The external load is calculated as the ratio of the external forces on the transmission to the weight of the unloaded transmission. In the validation of the proposed model, better results were attained than those obtained with the LuGre model when including an external load. Absolute identification errors ranged from 1.2% to a maximum of 11.1%; the model presents the best results at high external loads and low speeds.

The absolute errors were lower than those found with the LuGre model in all cases, obtaining errors up to 44% lower.

Despite not fully reproducing the friction behavior for the transmission, the proposed model constitutes a suitable alternative to the LuGre model for cable-driven transmissions and establishes a basis for further refinement.

Author Contributions: Conceptualization, G.T.-C. and J.-B.G.-M.; methodology, G.T.-C.; software, G.T.-C.; validation, G.T.-C. and J.-B.G.-M.; investigation, G.T.-C.; writing—original draft preparation, G.T.-C.; writing—review and editing, J.-B.G.-M.; visualization, G.T.-C.; supervision, J.-B.G.-M.; project administration, G.T.-C. All authors have read and agreed to the published version of the manuscript.

Institutional Review Board Statement: Not applicable.

Informed Consent Statement: Not applicable.

Data Availability Statement: The data presented in this study are available on request from the corresponding author.

Conflicts of Interest: The authors declare no conflict of interest.

References

1. Armstrong-Hélouvry, B.; Dupont, P.; De Wit, C.C. A Survey of Models, Analysis Tools and Compensation Methods for the Control of Machines with Friction. *Automatica* **1994**, *30*, 1083–1138. [CrossRef]
2. Boegli, M.; De Laet, T.; De Schutter, J.; Swevers, J. A Smoothed GMS Friction Model for Moving Horizon Friction State and Parameter Estimation. In Proceedings of the 2012 12th IEEE International Workshop on Advanced Motion Control (AMC), Sarajevo, Bosnia and Herzegovina, 25–27 March 2012; pp. 1–6. [CrossRef]
3. Nilkhamhang, I.; Sano, A. Adaptive Friction Compensation Using the GMS Model with Polynomial Stribeck Function. In Proceedings of the 2006 IEEE International Conference on Control Applications, Munich, Germany, 4–6 October 2006; pp. 1085–1090. [CrossRef]
4. Van Geffen, V. A Study of Friction Models and Friction Compensation. In *A Study of Friction Models and Friction Compensation*; Allen Institute for AI: Seattle, WA, USA, 2009; pp. 1–24.
5. Dupont, P.; Hayward, V.; Armstrong, B.; Altpeter, F. Single State Elastoplastic Friction Models. *IEEE Trans. Automat. Contr.* **2002**, *47*, 787–792. [CrossRef]
6. Swevers, J.; Al-Bender, F.; Ganseman, C.G.; Projogo, T. An Integrated Friction Model Structure with Improved Presliding Behavior for Accurate Friction Compensation. *IEEE Trans. Automat. Contr.* **2000**, *45*, 675–686. [CrossRef]
7. Lampaert, V.; Fassois, S.D.; Rizos, D.D.; Worden, K.; Engster, D.; Hornstein, A.; Parlitz, U. Measurement and Identification of Pre-Sliding Friction Dynamics. In *Nonlinear Dynamics of Production Systems*; Wiley-Vch: Weinheim, Germany, 2003; pp. 349–367.
8. Hayward, V.; Armstrong, B.S.R.; Altpeter, F.; Dupont, P.E. Discrete-Time Elasto-Plastic Friction Estimation. *IEEE Trans. Control. Syst. Technol.* **2009**, *17*, 688–696. [CrossRef]
9. Altpeter, F. *Friction Modeling, Identification*; École Polytechnique Fédérale de Lausanne: Lausanne, Switzerland, 1999; Volume 1988.
10. Kostić, D.; de Jager, B.; Steinbuch, M.; Hensen, R. Modeling and Identification for High-Performance Robot Control: An RRR-Robotic Arm Case Study. *IEEE Trans. Control. Syst. Technol.* **2004**, *12*, 904–919. [CrossRef]
11. Vargas, F.J.T.; De Fieri, E.R.; Castelan, E.B. Identification and Friction Compensation for an Industrial Robot Using Two Degrees of Freedom Controllers. In Proceedings of the ICARCV 2004 8th Control, Automation, Robotics and Vision Conference, 2004, Kunming, China, 6–9 December 2004; Volume 2, pp. 6–9. [CrossRef]
12. Kermani, M.R.; Patel, R.V.; Moallem, M. Friction Identification in Robotic Manipulators: Case Studies. In Proceedings of the Proceedings of 2005 IEEE Conference on Control Applications, 2005. CCA 2005, Toronto, ON, Canada, 28–31 August 2005; pp. 1170–1175. [CrossRef]
13. Swevers, J.; Verdonck, W.; De Schutter, J.; De Schutter, J. Dynamic Model Identification for Industrial Robots. *IEEE Control. Syst. Mag.* **2007**, *27*, 51–68. [CrossRef]
14. Susanto, W.; Babuška, R.; Liefhebber, F.; van der Weiden, T. Adaptive Friction Compensation: Application to a Robotic Manipulator. *IFAC Proc. Vol.* **2008**, *41*, 2020–2024. [CrossRef]
15. Kermani, M.R.; Patel, R.V.; Moallem, M. Friction Identification and Compensation in Robotic Manipulators. *IEEE Trans. Instrum. Meas.* **2007**, *56*, 2346–2353. [CrossRef]
16. Berger, E. Friction Modeling for Dynamic System Simulation. *Appl. Mech. Rev.* **2002**, *55*, 535. [CrossRef]
17. Olsson, H.; Åström, K.K.J.; de Wit, C.C.; Gäfvert, M.; Lischinsky, P. Friction Models and Friction Compensation. *Eur. J. Control.* **1998**, *4*, 176–195. [CrossRef]
18. Harnoy, A.; Friedland, B.; Cohn, S. Modeling and Measuring Friction Effects. *IEEE Control. Syst. Mag.* **2008**, *28*, 82–91. [CrossRef]
19. Kammerer, N.; Garrec, P. Dry Friction Modeling in Dynamic Identification for Robot Manipulators: Theory and Experiments. In Proceedings of the 2013 IEEE International Conference on Mechatronics (ICM), Vicenza, Italy, 27 February–1 March 2013; pp. 422–429.
20. Al-Bender, F.; Swevers, J. Characterization of Friction Force Dynamics Behavior and Modeling on Micro and Macro Scales. *IEEE Control. Syst. Mag.* **2008**, *28*, 64–81.
21. Åström, K.J.; Canudas-de-wit, C.; Augustin, C.; Amonton, D.C. Revisiting the LuGre Friction Model. *IEEE Control. Syst.* **2008**, *28*, 101–114.
22. Waiboer, R. Dynamic Modelling, Identification and Simulation of Industrial Robots. Ph.D. Thesis, Universiteit Twente, Enschede, The Netherlands, 2007.
23. Bittencourt, A.C.; Gunnarsson, S. Static Friction in a Robot Joint—Modeling and Identification of Load and Temperature Effects. *J. Dyn. Syst. Meas. Control.* **2012**, *134*, 051013. [CrossRef]

24. Bittencourt, A.C.; Wernholt, E.; Sander-Tavallaey, S.; Brogårdh, T. An Extended Friction Model to Capture Load and Temperature Effects in Robot Joints. In Proceedings of the 2010 IEEE/RSJ International Conference on Intelligent Robots and Systems, Taipei, Taiwan, 18–22 October 2010; pp. 6161–6167. [CrossRef]
25. Li, H.; Liu, W.; Wang, K.; Kawashima, K.; Magid, E. A Cable-Pulley Transmission Mechanism for Surgical Robot with Backdrivable Capability. *Robot. Comput. Integr. Manuf.* **2018**, *49*, 328–334. [CrossRef]
26. Morris, M.M.; Shoham, M.; Nahon, M. Applications and Theoretical Issues of Cable-Driven Robots. In Proceedings of the Florida Conference on Recent Advances in Robotics, Boca Raton, FL, USA, 21–22 May 2009; pp. 21–22.
27. Sari, A.; Saric, A.; Xiao, J.; Shi, J. Reducing Uncertainty in Robotic Surface Assembly Tasks Based on Contact Information. In Proceedings of the 2014 IEEE International Workshop on Advanced Robotics and its Social Impacts, Evanston, IL, USA, 11–13 September 2014; pp. 94–100. [CrossRef]
28. Phan, S.; Lioulemes, A.; Lutterodt, C.; Makedon, F.; Metsis, V. Guided Physical Therapy through the Use of the Barrett WAM Robotic Arm. In Proceedings of the 2014 IEEE International Symposium on Haptic, Audio and Visual Environments and Games (HAVE), Richardson, TX, USA, 10–11 October 2014; IEEE: Piscataway, NJ, USA, 2014; pp. 24–28.
29. Vicentini, F.; Pedrocchi, N.; Malosio, M.; Tosatti, L.M. SafeNet: A Methodology for Integrating General-Purpose Unsafe Devices in Safe-Robot Rehabilitation Systems. *Comput. Methods Programs Biomed.* **2014**, *116*, 156–168. [CrossRef]
30. Miyasaka, M.; Matheson, J.; Lewis, A.; Hannaford, B. Measurement of the Cable-Pulley Coulomb and Viscous Friction for a Cable-Driven Surgical Robotic System. In Proceedings of the 2015 IEEE/RSJ International Conference on Intelligent Robots and Systems (IROS), Hamburg, Germany, 28 September–2 October 2015; pp. 804–810. [CrossRef]
31. Miyasaka, M. Cable Driven Robots Hysteretic Cable Stretch, Cable-Pulley Network Friction, Fatigue Life, and Kinematics of Two-Arm Multi Staged Flexible Manipulator. Ph.D. Thesis, University of Washington, Seattle, WA, USA, June 2017. Available online: http://hdl.handle.net/1773/40641 (accessed on 28 February 2022).
32. Hannaford, B.; Rosen, J.; Friedman, D.W.; King, H.; Roan, P.; Cheng, L.; Glozman, D.; Ma, J.; Kosari, S.N.; White, L. Raven-II: An Open Platform for Surgical Robotics Research. *IEEE Trans. Biomed. Eng.* **2013**, *60*, 954–959. [CrossRef]
33. Choi, S.H.; Park, J.O.; Park, K.S. Tension Analysis of a 6-Degree-of-Freedom Cable-Driven Parallel Robot Considering Dynamic Pulley Bearing Friction. *Adv. Mech. Eng.* **2017**, *9*, 1–10. [CrossRef]
34. Lee, T.K.; Kim, C.Y.; Lee, M.C. Friction Analysis According to Pretension of Laparoscopy Surgical Robot Instrument. *Int. J. Precis. Eng. Manuf.* **2011**, *12*, 259–266. [CrossRef]
35. Charry, G.T.; Mendoza, J.-B.G. An Experimental Test Bench for Cable-Driven Transmission. *Machines* **2021**, *9*, 83. [CrossRef]
36. Townsend, W.T.; Guertin, J.A. Teleoperator Slave—WAM Design Methodology. *Ind. Robot. Int. J.* **1999**, *26*, 167–177. [CrossRef]
37. Carl Stahl Sava Industries. *Design Guide for Cable SolutionsTM*; Technical Report: Suessen, Germany, 2010.
38. Werkmeister, J.; Slocum, A. Theoretical and Experimental Determination of Capstan Drive Stiffness. *Precis. Eng.* **2007**, *31*, 55–67. [CrossRef]
39. Merry, R.J.E. *Wavelet Theory and Its Applications—A Literature Study*; Eindhoven University of Technology: Eindhoven, The Netherlands, 2005.
40. Giaouris, D.; Finch, J.W.; Member, S.; Ferreira, O.C.; Member, S.; Kennel, R.M.; Member, S.; El-murr, G.M. Wavelet Denoising for Electric Drives. *IEEE Trans. Ind. Electron.* **2008**, *55*, 543–550. [CrossRef]
41. Misiti, M.; Misiti, Y.; Oppenheim, G.; Poggi, J.-M. Wavelet ToolboxTM User's Guide. Available online: https://www.mathworks.com/help/pdf_doc/wavelet/wavelet_ug.pdf (accessed on 28 February 2022).